Energy Dissipation in Flexural Failure Process of Reinforced Concrete Beams

By

Kiyoshi OKADA*, Wataru KOYANAGI**
and Keitetsu ROKUGO*

(Received December 27, 1979)

Abstract

The energy dissipation in the flexural failure process of RC (reinforced concrete) beams was related to ductile behavior.

RC beams with three reinforcement ratios (0.83%, 2.25% and 6.18%) were loaded beyond the peak load to investigate the role of reinforcement and concrete in the energy dissipation during the flexural failure process of the beams. The relationship between the plastic rotation capacity and the energy dissipation in RC beams was discussed. The amount of acoustic emissions was related to the energy dissipation.

The energy dissipated in the reinforcing bars during yield W_{is} was determined from the irrecoverable deformation of the reinforcement. As the reinforcement ratio increased, the energy dissipated in the concrete W_{ic} increased, and the energy dissipated in the reinforcement W_{is} decreased. After the yield of the reinforcement, W_{is} increased with the beam displacement, then stopped increasing at a certain displacement, after which the energy was dissipated only in the concrete. The energy dissipation in the range from the onset of the reinforcement yielding to the end of the energy dissipation in the reinforcement was proposed as an index to evaluate the plastic rotation capacity of the steel hinging of RC beams.

1. INTRODUCTION

If structures were ductile enough to absorb energy, their collapse during a major earthquake could be avoided and human life saved. Thus, ductility is one of the most important properties of members and structures.

In this investigation, energy dissipation in the flexural failure process of RC beams (reinforced concrete beams) is related to ductile behavior. In the failure process of RC beams under flexure, the work done, W_i, to the beams due to externally applied loads is divided into W_r and W_i. W_r is the strain energy stored in the beams, and W_i is the dissipated energy consumed in the beams. This dissipated energy, W_i, con-

* Department of Civil Engineering at Kyoto University
** Department of Civil Engineering at Gifu University

sists of two components, W_{ic} and W_{is}. W_{ic} is the energy dissipated in the concrete mainly as a surface energy, and W_{is} is the energy dissipated in the plastic deformation of the reinforcement after the yield.

From tests of RC beams with different reinforcement ratios, which were loaded beyond the peak load, the energies dissipated in the reinforcement and concrete were calculated, and the role of the reinforcement and concrete in the energy dissipation was considered. The dissipated energy was related to the displacement and fracture phenomena of the RC beams. The number of AE (Acoustic Emissions) generations during the failure process of the beams was counted, and then the relationship between the number of AE generations and the energy dissipation in the reinforcement and concrete was investigated. The method of evaluating the plastic rotation capacity of RC beams, based on the measured plastic curvature and the dissipated energy in the reinforcement, was employed.

2. EXPERIMENTAL PROCEDURES

2.1 Test Program and Fabrication of Beams

Three RC beams with different reinforcement ratios, 0.83%, 2.53% and 6.18%, were used in order to change the relation between the yield of the reinforcement and the crushing of the concrete for the RC beams under flexure. The first reinforcement ratio, 0.83%, is nearly a balanced one in the working stress design. The third one, 6.18%, represents an over-reinforcement even in the ultimate strength design. In this case, the crushing of the concrete occurs without the yield of the reinforcement. The three RC beams were reinforced with three sizes of deformed reinforcing bars, 10 mm, 16 mm, and 25 mm in nominal diameter, respectively. Therefore, hereafter these beams will be called B10, B16 and B25.

The dimension of the beam specimens was $10 \times 20 \times 160$ cm. As shown in Fig. 1, stirrups were used to prevent shear failure. The stirrups (6 mm diameter bars) were spaced so that the stress in the stirrups at the maximum shear load was less than the yield strength of the bars. The concrete cover for the reinforcement was 2.3 cm.

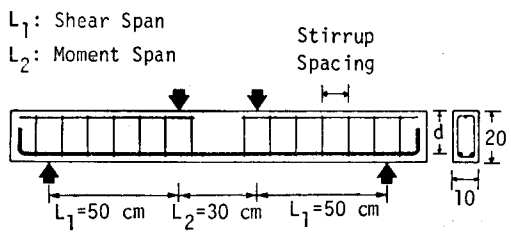

Fig. 1. Reinforcement in Beam.

Table 1. Effective Depth and Stirrup Spacing.

Beam	Stirrup Spacing cm	Effective Depth d, cm
B10	10.0	17.2
B16	10.0	16.9
B25	7.5	16.4

Table 2. Mechanical Properties of Reinforcing Bars.

Reinforcing Bar	Nominal Dimensions: Diameter mm	Nominal Dimensions: Cross-Sec. Area cm^2	Yield Load P_y, t	Yield Strength f_y, kg/mm^2	Peak Load P_p, t	Tensile Strength f_u, kg/mm^2
Def. Bar (D10)	9.53	0.713	2.69	37.7	3.97	55.7
Def. Bar (D16)	15.9	1.986	7.06	35.5	10.49	52.8
Def. Bar (D25)	25.4	5.067	23.0	45.4	32.7	64.5
Plain Bar	6.0	0.283	1.20	42.4	1.32	46.6

Table 3. Mix Proportion.

Water-Cement Ratio	Sand-Aggr. Ratio	Mix Materials, kg/m^3: Water	Cement	Sand	Gravel 5~15mm	Slump cm
0.68	0.42	192	283	770	1084	4

The effective depth and the spacing of the stirrups for each beam are presented in Table 1. The mechanical properties of the reinforcing bars are given in Table 2. The strain in the reinforcing bars at the yield was measured with plastic strain gages (gage length: 5 mm).

The concrete was made from normal portland cement, crushed sandstone (specific gravity: 2.64, maximum size: 15 mm), and river sand (specific gravity: 2.61, fineness modulus: 3.0). The mix proportion of the concrete and the measured slump are given in Table 3.

All beam specimens were cast at the same time. After unmolding, they were cured in the testing room and loaded at the testing age of from 41 to 43 days. The average compressive strength of concrete, f_c, calculated from 7 cylindrical specimens ($\phi 10 \times 20$ cm), was 316 kg/cm^2.

2.2 Loading and Measuring of Displacement

The RC beams were loaded at the span of 130 cm, as illustrated in Fig. 1. Several

cycles of loading and unloading were carried out, increasing the maximum load-point displacement with each repetition by a constant rate (approximately 5 mm/min.). The minimum load level after each unloading was between 0.2 t and 0.4 t.

The displacement (deflection) of the beams, the strain in the steel bars and concrete, and the number of AE generations were measured.

Five dial-gage type electric displacement meters were used to measure the displacement (deflection) of the beams. As shown in Fig. 2, the meters were fixed to a supporting bar, which was directly attached to the beams at two points over the loading span to eliminate any possible error in the measured displacement due to the seating of the support points and the deformation of the loading machine, etc. One of the attaching points was rotatable, and the other was rotatable and slidable. An X−Y recorder recorded the relation between the load-point displacement, which was detected with a displacement meter under one of the load-points, and the load, which was detected with a load cell. Hereafter, this relationship will be called the load-displacement diagram.

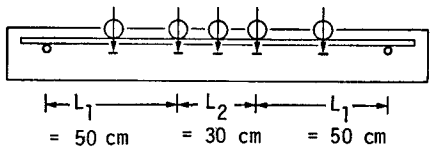

Fig. 2. Equipment for Measuring Deflection.

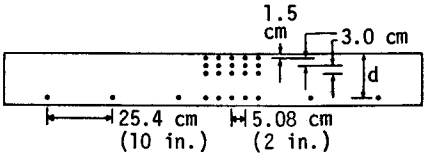

Fig. 3. Gage Points on Beam.

The change in the lengths between the gage points, which were glued at 25.4 cm (10 in.) horizontal intervals at the same height on the side surface of the concrete, as shown in Fig. 3, were measured with a Whittemore strain meter (least count: 0.025 mm, gage length: 25.4 cm) to determine the deformation of the reinforcing bars along the axis of the beams. When the deformation between the marked points became greater than 1.3 mm due to cracking, a caliper (least count: 0.1 mm) was used to measure the deformation instead of the Whittemore strain meter.

The change in the lengths between the gage points, which were placed at 5.08 cm (2 in.) horizontal intervals in four lines and five columns as shown in Fig. 3, was measured with a 5.08 cm (2 in.) length Whittemore strain meter in order to find the position of the neutral axis and the strain distribution across the depth of the beams. The load-point displacement was kept constant during the measuring. The strain in the reinforcement was measured at the center of the moment span (constant moment region) and under the load-points with electric resistance strain gages (gage length: 5 mm) glued to the reinforcing bars. The strain in concrete was measured at both the compression fiber (top surface) and the tension fiber (bottom surface) inside the

moment span with electric resistance strain gages (gage length: 67 mm).

The number of AE generations was counted with a pickup, which was attached at the center of the side surface of the beams. The AE's had a frequency of from 20 to 300 kHz, were amplified to 60 dB, and were over 100mV. The details of the AE detecting method are reported in Reference [1].

2.3 Calculation of Energy

The work done, W_t, which is applied to the specimen by an external load, is transformed into reversible elastic strain energy, W_r, which is stored in the specimen, and into irreversible dissipated energy, W_i, which is absorbed in the specimen. The dissipated energy W_i was divided into W_{ic} and W_{is}, and then calculated. W_{ic} is the energy dissipated in the concrete as surface energy, and W_{is} is the energy dissipated at the yield of the steel. Each energy was calculated in the following way. The area OUQ, defined by the loading curve OU and the displacement axis in Fig. 4, indicates the work done (W_t), applied to the beam up to the unloading point U in the load-displacement diagram.

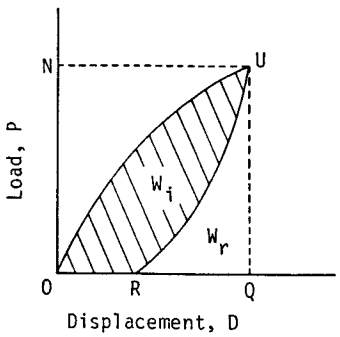

Fig. 4. Calculation of Energy.

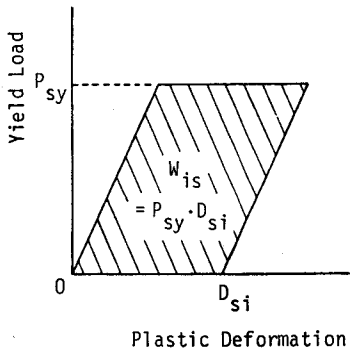

Fig. 5. Dissipated Energy in Steel.

The dissipated energy W_i, corresponding to the unloading point U, is calculated from the area OUR, which is defined by both the loading curve OU up to the point U, and the unloading curve UR. The reversible elastic strain energy W_r is given by the area RUQ under the unloading curve UR. In analyzing the data, the enveloping curve connecting the unloading points was used as the loading curve. These areas were measured with a planimeter.

As illustrated in Fig. 5, the dissipated energy at the yield of the reinforcement, W_{is}, was calculated from the product of P_{sy}, the yield load of the reinforcing bars, by D_{si}, the irrecoverable deformation measured along the beam axis at the position of the reinforcement after unloading. The work hardening of the reinforcing bars was

not considered in this study. The details of the calculation of W_i, are described in Section 4.

The dissipated energy in the concrete, W_{ic}, was calculated by subtracting W_{is}, the dissipated energy in the reinforcement, from W_i, the total dissipated energy in the beam. That is, $W_{ic}=W_i-W_{is}$. W_{ic} may include not only the energy dissipated as surface energy in the compression and the tension zones of the concrete, but also the energy dissipated in the bond fracture between the reinforcing bars and concrete.

3. LOAD-DISPLACEMENT DIAGRAM

The load-displacement diagrams of the RC beams, B10, B16 and B25, are given in

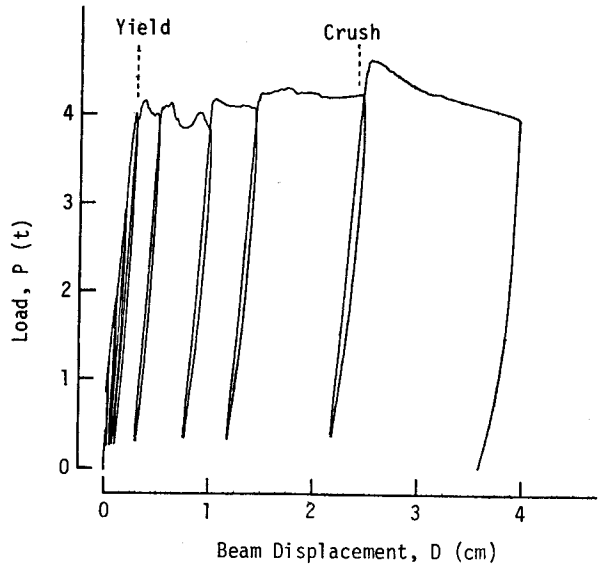

Fig. 6. Load-Displacement Diagram of Beam B10.

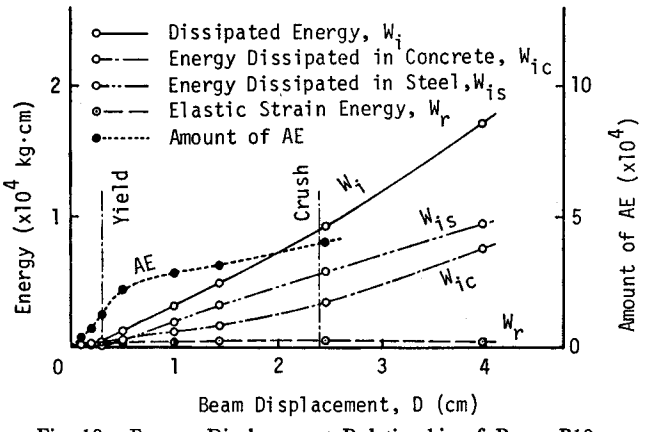

Fig. 10. Energy-Displacement Relationship of Beam B10.

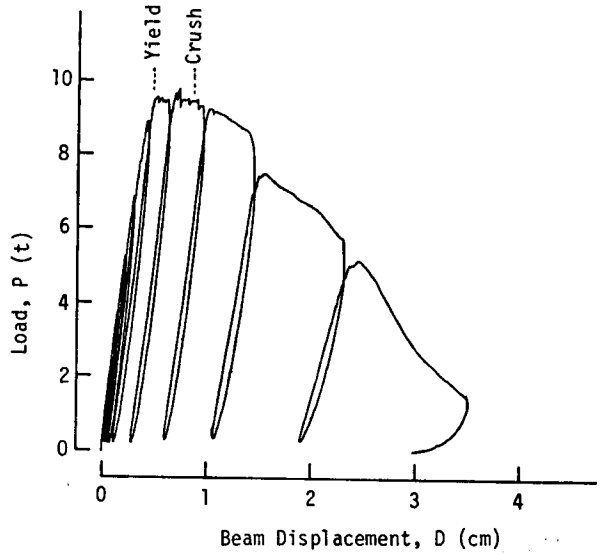

Fig. 7. Load-Displacement Diagram of Beam B16.

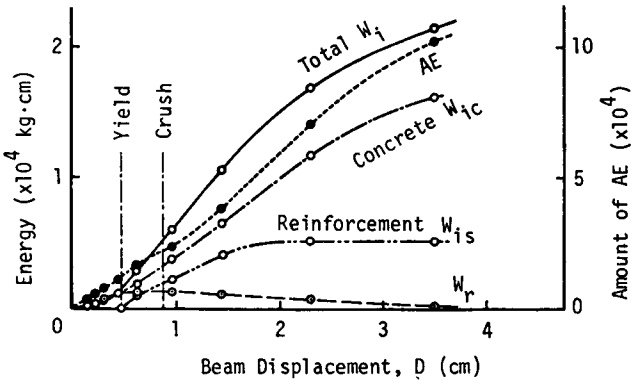

Fig. 11. Energy-Displacement Relationship of Beam B16.

Figs. 6, 7 and 8, which were displayed on the X−Y recorder. In general, the load-displacement diagrams of the RC beams in flexure are characterized by a crack initiation, a yield of reinforcement, a strength failure (peak load), a crushing of the concrete in the compression zone and post-failure region, etc.

The initial points of the yield of the reinforcement and of the crushing in the concrete are marked in Figs. 6, 7 and 8. The initial point of the steel yielding was defined as a critical point, where the strain in the reinforcing bars measured with strain gages began to increase suddenly. The critical strain was $2100 \sim 2200 \times 10^{-6}$. It was identical with the strain at the beginning of yield in the tension test of the rein-

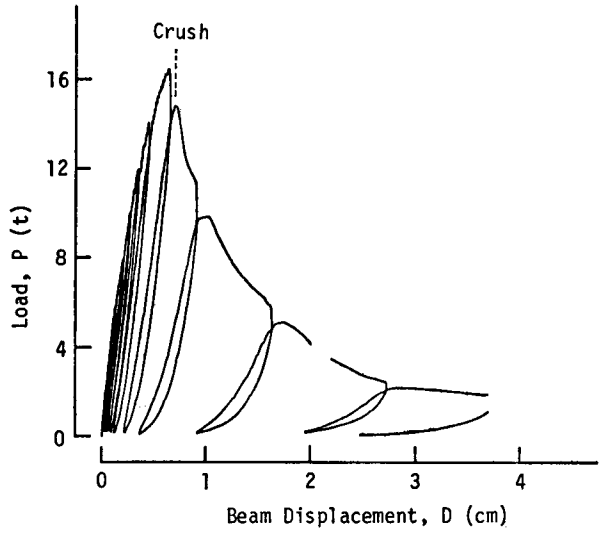

Fig. 8. Load-Displacement Diagram of Beam B25.

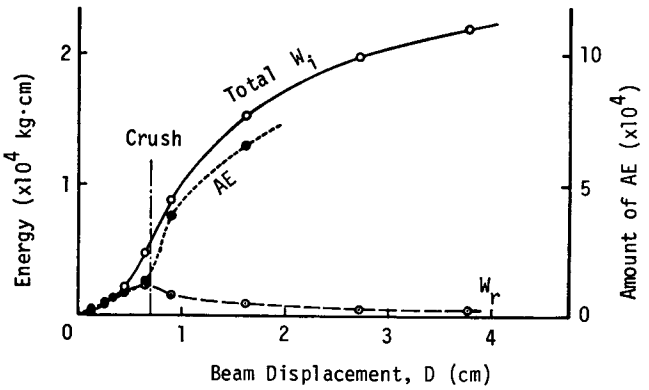

Fig. 12. Energy-Displacement Relationship of Beam B25.

forcing bars. The beginning of crushing in the concrete was determined by observation with the naked eye.

In the case of Beam B10 with low reinforcement ratio, after the reinforcing bars reached the yield strength at a displacement of 0.30 cm, the beam displacement increased greatly with a small increase in load until the onset of crushing in the concrete at a displacement of 2.40 cm. After the peak load point, the load-displacement relationship curved downward.

In the case of Beam B16, the reinforcement began to yield at a displacement of 0.48 cm, and then the concrete began to crush in compression at a displacement of 0.83 cm. After the onset of crushing, the rate of load decrease was accelerated with

Table 4. Yield Moment and Peak Moment of Beams.

Beam	Yield Load P_y, t	Yield Moment M_{ym}, t·m	Peak Load P_p, t	Peak Moment M_p, t·m	Cal. Yield Moment M_{yc}, t·m	$\frac{M_{ym}}{M_{yc}}$
B10	4.1	1.03	4.6	1.15	0.88	1.17
B16	9.5	2.38	9.6	2.40	2.07	1.15
B25	—	—	16.3	4.08	—	—

the progress of concrete failure.

In the case of Beam B25 with over-reinforcement, the reinforcing bars did not yield, and the displacement at the peak load was 0.65 cm. The load-displacement curve after compression failure was the steepest. The displacement at the onset of concrete crushing was 0.70 cm.

The effect of the reinforcement ratio on the ductility of each beam is described in Section 7.

The yield load of each beam, P_y, which was measured at the initiation of the yield of the reinforcement, the peak load, P_p, and the moments corresponding to each load are presented in Table 4. The yield moment of each beam, M_{yc}, was calculated from the following formula using f_{ty}, the yield strength of the deformed reinforcing bars, and f_c, the compression strength of the concrete:

$$M_{yc} = pf_{ty}\left(1 - \frac{pf_{ty}}{2f_c}\right)Bd^2 \tag{5.1}$$

where, p is the reinforcement ratio, B is the width of the beam, and d is the effective depth.

M_{yc} of Beam B25 was not calculated by the above formula, since the reinforcement did not yield. The measured yield moments, M_{ym}, of Beams B10 and B16 are about 15% greater than the calculated yield moments, M_{yc}. It has been reported that small size model beams reinforced with deformed bars give this result [2]. One of the reasons may be that the strain in the reinforcement near the cracks in the concrete became large enough for work hardening, because of the higher bond strength of the deformed bars. The details of these reasons should be examined further. Since the purpose of this investigation is to roughly separate the dissipated energies in the concrete and in the steel during the failure process of the RC beams in flexure, the effect of the work hardening of the reinforcement on the calculation of the dissipated energy was not taken into consideration.

4. DEFORMATION AND ENERGY DISSIPATION

The total deformation of the reinforcement was measured on the concrete surface along the reinforcement. That is, the deformation was measured at five sections, which were marked with small plugs on the concrete surface at intervals of 25.4 cm (10 in.). Therefore, the total gage length was 127 cm within the beam span of 130 cm.

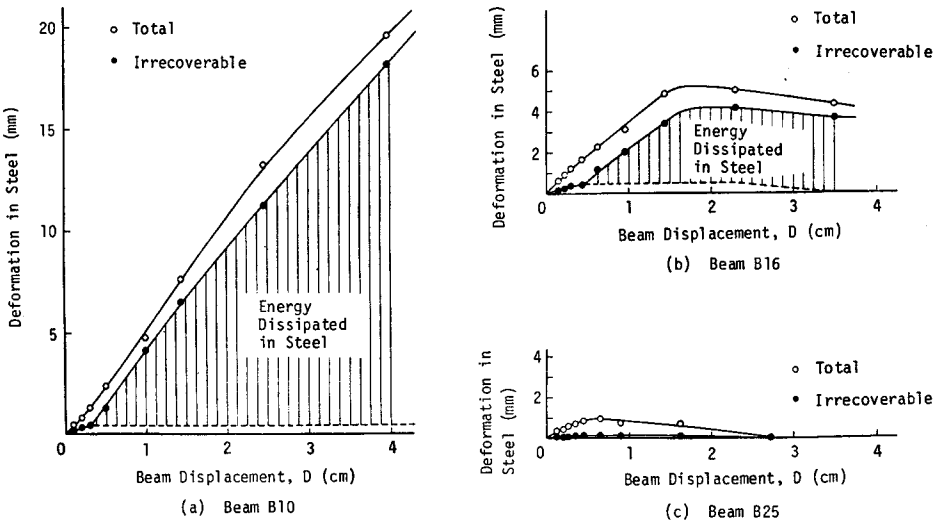

Fig. 9. Total Deformation of Reinforcement.

Fig. 9 shows the relationship between the beam displacement and the total deformation of the reinforcement in Beams B10, B16 and B25. In these figures, the circle shows the deformation of the reinforcement at an unloading point. The black point shows the irrecoverable deformation at the minimum load after unloading, relating to the beam displacement at the previous unloading point.

In the case of Beam B10, the irrecoverable deformation increased rapidly and constantly with the beam displacement after the yield of the reinforcement. The irrecoverable deformation just before the yield was 0.43 mm. This may include the elastic deformation due to the minimum load after unloading. Therefore, the irrecoverable deformation just before the yield was subtracted from the irrecoverable deformation at each unloading point, when the dissipated energy in the reinforcement, W_{is}, was calculated. W_{is} was calculated by multiplying the yield load of the reinforcements by the irrecoverable deformation, which is indicated by the oblique lines in Fig. 9(a).

Also for Beam B16, the irrecoverable deformation just before the yield was subtrac-

ted from the irrecoverable deformation at the unloading points in the calculation of W_{is}. In the region above a beam displacement of 2 cm in Fig. 9 (b), the load decreased remarkably and the load at the final unloading point was about one seventh of the peak load. Moreover, the elastic deformation was almost completely recovered when the beam displacement was large. Therefore, the irrecoverable deformation without any subtraction was used in the calculation of W_{is} at the final unloading point. As seen from Fig. 9 (b), there was a critical point after the peak load point, where the total deformation of the reinforcement began to decrease. This point coincided with the point where the irrecoverable deformation of the reinforcement stopped increasing.

Although the total deformation of the reinforcement in Beam B25 at the peak load point was 0.96 mm, the total deformation at the final stage was nearly zero, because the reinforcement did not yield.

The elastic strain energy, W_r, the total dissipated energy, W_i, the energy dissipated in the reinforcement, W_{is}, and the energy dissipated in the concrete, W_{ic}, of each beam are related to the beam displacements at the unloading points in Figs. 10, 11 and 12. The onsets of the reinforcement yield and of the concrete crushing are marked in these figures.

As seen from Fig. 10 related to Beam B10, the increase in the total dissipated energy, W_i, after the yield of the reinforcement was large. Especially, the dissipated energy in the reinforcement, W_{is}, remarkably increased in proportion to the beam displacement after the yield. Then, W_{is} exceeded W_{ic}, the dissipated energy in the concrete, at a displacement of 0.6 cm, which was about twice the displacement at the yield. W_{ic} existed from the beginning of the loading, and constantly increased as the beam displacement increased.

It can be seen from Fig. 11 that W_{is} of Beam B16 increased after the yield of the reinforcement, as did Beam B10. However, it became constant at a displacement of 1.7 cm (which was four times larger than that at the initiation of yielding) due to the decreasing load. After this point, energy was dissipated only in the concrete. W_{ic} was always greater than W_{is}, and W_r decreased as the load-carrying capacity decreased.

The reinforcement of Beam B25 did not yield, as shown in Fig. 12. Therefore, only the concrete contributed to the energy dissipation. W_r was maximum at the peak load, just before the beginning of the concrete crushing, and then decreased with a decrease in the load.

It can be seen from the comparison of Figs. 10, 11 and 12 that an RC beam with a high reinforcement ratio tends to have a relatively large W_{ic} and small W_{is}. Before the yield of the reinforcement, energy was consumed only in the concrete. The peak loads, depending on the reinforcement ratios, were so different that there

was also a large difference in the total dissipated energies at the yielding of the reinforcement and at the crushing of the concrete. However, when the beam displacement was sufficiently large, about 4 cm, and the load decreased, W_i was about 2×10^4 kg·cm for the three beams, and did not depend on the reinforcement ratios.

5. NEUTRAL AXIS

Fig. 13 shows the strain distribution in the moment span, which was measured by using the gage points (2 in. spacing×4 lines) on the side surface of the beam. The strain distributions in Fig. 13 were almost linear, so that the assumption of the plain sections seemed to be satisfied. Only when the displacement of Beam B10 was great, was the strain distribution in the concrete not linear at the reinforcement level. The neutral axis positions calculated from Fig. 13 are related to the beam displacements in Fig. 14. The open points in Fig. 14 show the beam deflection where the strain distribution in Fig. 13 was measured.

The neutral axis of Beam B16 rose with the beam displacement after the yield of the reinforcement, and reached its maximum level at the beginning of the crushing in the concrete. After that, spalling in the concrete due to failure in the compression caused the neutral axis to descend toward the reinforcement in order to maintain the balance of the moment.

In the case of Beam B10 with the low reinforcement ratio, the neutral axis rose immediately after the yield of the reinforcement. The depth of the compression zone was so small that the change in position of the neutral axis and the depth of the

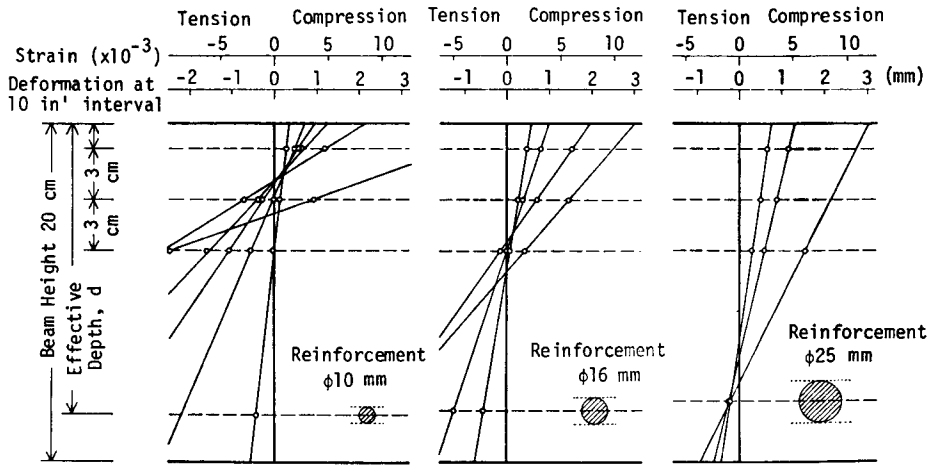

(a) Beam B10 (b) Beam B16 (c) Beam B25

Fig. 13. Strain Distribution in Moment Span.

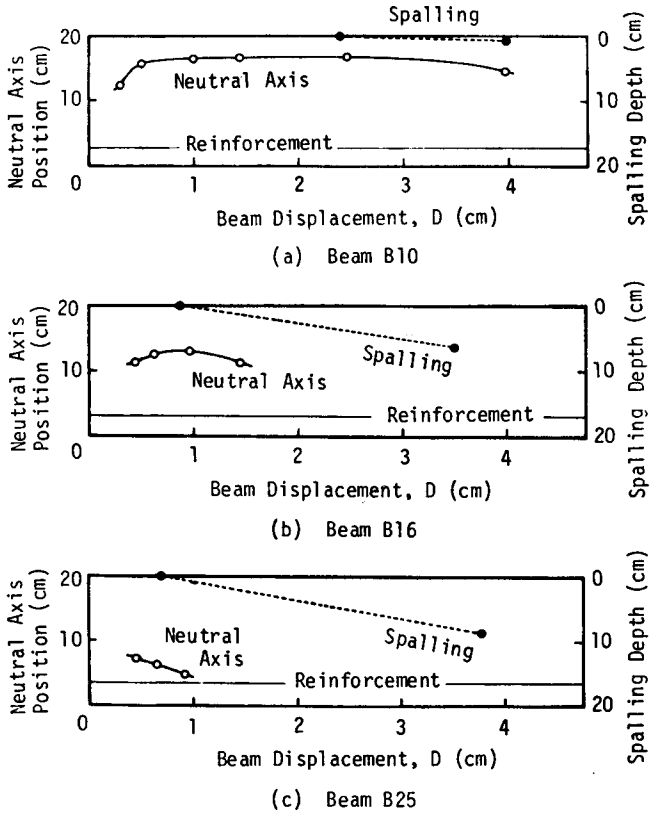

Fig. 14. Neutral Axis Position and Spalling Depth.

spalling were small, even when the displacement was large.

Because Beam B25 was over-reinforced, the neutral axis was always below the center line of the cross-section. The depth of the compression zone increased, and the neutral axis approached the reinforcing bars as the beam displacement increased. The depth of concrete spalling was very large.

6. ACOUSTIC EMISSION

The relationship between the number of AE generations and the beam displacement is indicated in Figs. 10, 11 and 12 by the dotted line.

In the case of Beam B10, the number of AE generations rapidly increased before the yield of the reinforcement. When the beam displacement exceeded 0.5 mm after the yield point, the rate of AE generations became slow. This tendency probably reflects the increase in the size and number of cracks in the concrete and of the bond cracks between the concrete and steel.

For Beam B25, the number of AE generations began to increase suddenly at the initiation of concrete crushing. It seems that, for the most part, the AE's are generated during the compression failure of the concrete. When the beam displacement became large, the AE's could not be measured because the pickup fell off due to the crushing of the concrete.

The number of AE generations was small at the beginning of the loading, and then increased constantly until the yielding of the reinforcement in Beams B10 and B16, or until the crushing of the concrete in Beam B25. By comparing the number of AE generations with the dissipated energies, it can be seen that the shape of the curve of AE generations was similar to that of the energy dissipated in the concrete, W_{ic}. This fact suggests that most of the AE's were generated in the concrete.

7. PLASTIC ROTATION CAPACITY

The change in curvature from the beginning of the reinforcement yield to the observed crushing of the concrete, or to the equivalent gage-measured strain in the compression fiber (for example, 3000×10^{-6}), has been used to evaluate the plastic rotation capacity, that is to say, the capacity of the RC beams to act as a plastic hinge. Also, the deflection of the beams after the yield has been used to evaluate this capacity [3]. Besides such a steel hinge effect, which is caused by the yield of the reinforcement, there is also a concrete hinge effect, which is caused by the crushing of the concrete in the compression zone. Because the capacity of the latter is small, only the steel hinge effect has been investigated.

As seen from Figs. 6 and 7, the load was almost constant between the yield point and the concrete crushing point. As described above, the change in deflection or curvature, which is calculated from the strain distribution in Fig. 13, from the yield point of the reinforcement to the crushing point of the concrete can be used to evaluate the plastic rotation capacity of the beams. The dissipated energy during the above period may be directly related to the plastic rotation.

When the flexural yield moment, M_y, causes the plastic curvature, Φ_p, in the constant moment span, L_2 in Fig. 1, then the dissipated energy, W_i, due to the plastic rotation is as follows:

$$W_i=\int_0^{L2} M_y\Phi_p dx \qquad (5.2)$$

The curvature after the yield of the reinforcement was observed to be concentrated in the moment span, L_2. If the plastic curvature Φ_p can be assumed macroscopically uniform, the plastic curvature Φ_p and the dissipated energy W_i are related by the following equation:

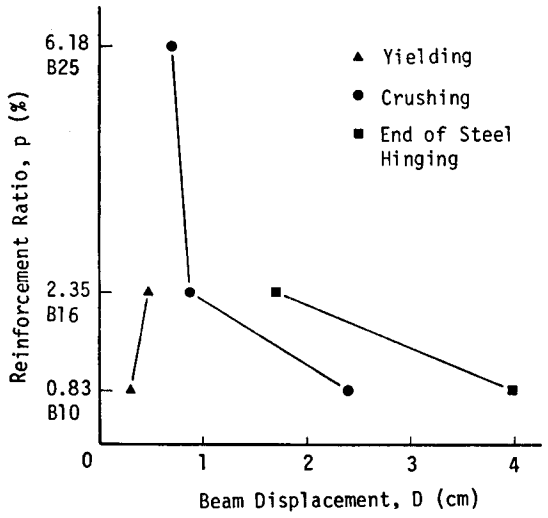

Fig. 15. Reinforcement Ratio and Beam Displacement.

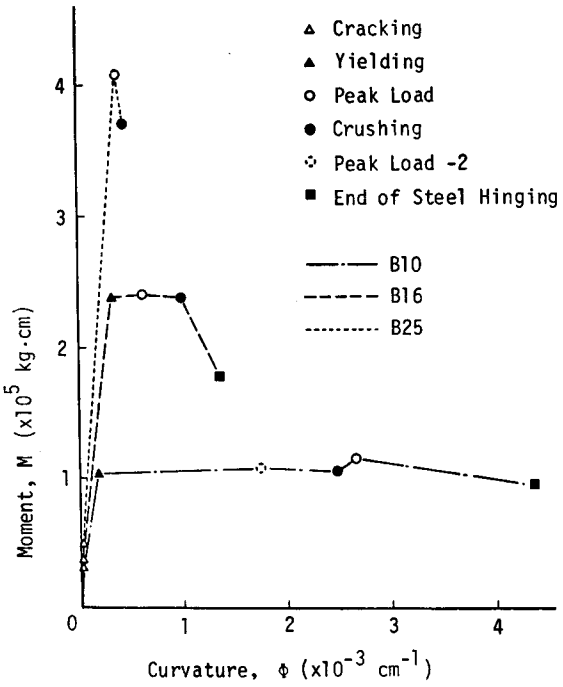

Fig. 16. Moment and Curvature.

$$\Phi_p = W_i / M_y L_2 \qquad (5.3)$$

The starting point of the plastic rotation in the steel hinge effect is the starting point of the yield in the reinforcement. The initiation of the concrete crushing has been ordinarily used as the end point. The point where the energy dissipation in the reinforcement stops could also be used as the end point of the steel hinging. Fig. 15 shows the relationship between the reinforcement ratio and the beam displacement at the onset of the reinforcement yield, at the initiation of the concrete crushing, and at the end of the steel hinge effect defined above. The relationship between the moment and the curvature is given in Fig. 16. In this figure, the point of peak load-2 for Beam B10 is not the actual peak load point. However, it is treated as the peak load hereafter, because Fig. 6 shows that it was not affected by the loading rate and the load repetitions. The difference between the load at this point and the measured peak load was small. As seen from these Figures, the beam displacement and the curvature at the onset of the reinforcement yield increased slightly as the reinforcement ratio increased. However, the displacement and the curvature at the initiation point of the concrete crushing, or the end point of the steel hinging, decreased drastically with the increase in the reinforcement ratio. Consequently, the displacement or the curvature resulting from the plastic rotation decreased as the reinforcement ratio increased. Though the moment carrying capacity of Beam B10 with the low reinforcement ratio did not decrease between the concrete crushing point and the end of the steel hinging, the moment carrying capacity of Beam B16 with the higher reinforcement ratio did decrease slightly.

Assuming the flexural moment carrying capacity after the reinforcement yield point to be constant, the plastic curvature Φ_p was calculated by Equation (5.3) from the dissipated energy W_i for two different regions: One from the yield point of the reinforcement to the crushing point of the concrete (named as Region-1), and the other from the yield point of the reinforcement to the end point of the steel hinging (named as Region-2). The measured plastic curvature, Φ_{pm}, in Fig. 16 and the cal-

Table 5. Dissipated Energy and Plastic Curvature.

Beam	Region	Dissipated Energy W_i, $\times 10^4$kg·cm	Calculated Plas. Curv. Φ_{pc}, $\times 10^{-3}$/cm	Measured Plas. Curv. Φ_{pm}, $\times 10^{-3}$/cm
B16	1	0.86	2.8	2.3
	2	1.68	5.4	4.3*
B16	1	0.39	0.6	0.7
	2	1.16	1.6	1.1

* More than 4.3

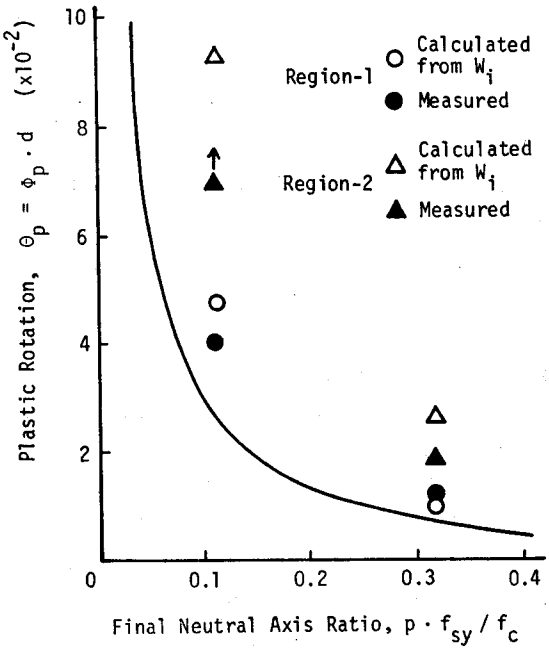

Fig. 17. Plastic Curvature and Final Neutral Axis Ratio.

culated curvature, Φ_{pc}, are presented in Table 5. The values of Φ_{pm} and Φ_{pc} seem to be in agreement with each ether, in spite of the rough assumption regarding the duration of the plastic hinge effect and the lack of accuracy in Fig. 16. It can be concluded that the plastic rotation capacity can be directly related to the energy dissipated during rotation. The plastic rotation capacity for Beam B10 was greater than that for Beam B16, and the capacity for Region-2 was twice that for Region-1.

It has been pointed out that the plastic rotation capacity is related to the final ratio of the neutral axis [3]. The results in Table 5 are marked in Fig. 17, which is a trial calculation of the above described relation by Koyanagi [4], made by assuming the stress-strain curves of both steel and concrete to be bi-linear. In Fig. 17, the plastic curvature is normalized in terms of rotation as: $\Theta_p = \Phi_p$ d, where d is the effective depth. The curvature calculated from the dissipated energy, and the measured plastic curvature for Region-1 seem to be almost in agreement with the results in Fig. 17. The plastic rotation capacity for Region-2, (which ends at the point where the energy dissipation in the reinforcement stops), is about twice that for Region-1. The meaning of this phenomenon should be investigated further with relation to the moment redistribution in actual structures and to the load carrying capacity. The dissipated energy for Region-2 may be the parameter of the energy dissipation due to the plastic rota-

tion in the steel hinge. Therefore, the dissipated energy would be a useful means to study the rotation capacity of the plastic hinge and the failure process of RC beams under flexure.

8. CONCLUSION

RC beams with three reinforcement ratios (0.83%, 2.25% and 6.18%) were tested to investigate the role of reinforcement and concrete in energy dissipation during the flexural failure process of the beams. The relationship between the plastic rotation capacity and the energy dissipation in the RC beams has been discussed in this paper.

The following results were obtained:

(1) The work done on the RC beams by an external load, W_i, was separated into the reversible strain energy, W_r, and the dissipated energy, W_i. The energy dissipated in the reinforcing bars during the yield, W_{is}, was determined from the irrecoverable deformation of the reinforcement. The energy dissipated in the concrete, W_{ic}, was calculated by subtracting W_{is} from W_i. The quantitative results show that as the reinforcement ratio increased, the energy dissipated in the concrete increased, and the energy dissipated in the reinforcement decreased.

(2) The neutral axis position was calculated from the concrete strain distribution in the moment span. In the case of a beam with a low reinforcement ratio, the neutral axis rose with an increase in the flexural moment and then descended after the concrete crushing. In general, the greater the reinforcement ratio, the lower the position of the axis. Especially, in the case of an over-reinforced beam, the neutral axis approached the reinforcing bars. A RC beam with a high reinforcement ratio tended to have relatively large W_{ic}.

(3) After the yield of the reinforcement, the energy dissipated in the reinforcing bars increased with the beam displacement. It then stopped increasing at a certain displacement, after which the energy was dissipated only in the concrete.

(4) The relation between the number of AE generations and the beam displacement was similar to the relationship between the dissipated energy (especially the energy dissipated in the concrete) and the beam displacement.

(5) The plastic rotation capacity of the RC beams decreased as the reinforcement ratio or the final neutral axis ratio increased. Both the plastic curvature calculated from the dissipated energy, and the measured plastic curvature, were almost in agreement with the plastic curvature. This was computed on the basis of the simplified assumption that the stress-strain relationship is bilinear for both concrete and reinforcement. The plastic curvature or the energy dissipation in the range from the onset of the reinforcement yielding to the end of the energy

dissipation in the reinforcement would be a useful index to evaluate the plastic rotation capacity of steel hinging.

References

1) Niwa, Y., Kobayashi, S. and Otsu, M., "Studies of Acoustic Emissions in Concrete Structures", Proc. JSCE, No. 261, 1977. 5 (101-112) [in Japanese].
2) Mattock, A. H., Kriz, L. B. and Hognestad, E., "Rectangular Concrete Stress Distribution in Ultimate Strength Design," Jour. ACI, **32**-8, 1961. 2 (875-928).
3) Yamada, M., "Drehfähigkeit Plastischer Gelenke in Stahlbeton Balken," Beton ud. Stahlbau, **27**-4, 1958. 4 (85-91).
4) Koyanagi, W., "Plastic Hinging in Concrete Members," Con. Jour. JCI, **15**-5, 1977. 5 (1-10) [in Japanese].